Effects of solutal convection on the dissolution of GaSb into InSb melt and solute transport mechanism in InGaSb solution: Numerical simulations and in-situ observation experiments

Effects of solutal convection on the dissolution of GaSb into InSb melt and solute transport mechanism in InGaSb solution: Numerical simulations and in-situ observation experiments

G.Rajesh[a)], M.Arivanandhan[a)], N.Suzuki[a)], A.Tanaka[a)], H.Morii[a)], T.Aoki[a)], T.Koyama[a)], Y.Momose[a)], T.Ozawa[b)], Y.Inatomi[c)], Y.Takagi[d)], Y.Okano[d)] and Y.Hayakawa[a), *]

[a)] *Research Institute of Electronics, Shizuoka University, 3-5-1 Johoku, Naka-ku, Hamamatsu, Shizuoka 432-8011, Japan*

[b)] *Department of Electrical Engineering, Shizuoka Institute of Science and Technology, 2200-2 Toyozawa, Fukuroi, Shizuoka 437-8555, Japan*

[c)] *Institute of Space and Astronautical Science, Japan Aerospace Exploration Agency, 3-1-1 Yoshinodai, Sagamihara, Kanagawa 229-8510, Japan*

[d)] *Graduate School of Engineering Science, Osaka University, 1-3 Machikaneyama, Toyonaka, Osaka 560-8531, Japan*

Corresponding author:

Yasuhiro Hayakawa

Research Institute of Electronics, Shizuoka University, 3-5-1 Johoku, Naka-ku,

Hamamatsu 432-8011, Japan

Tel/Fax: +81-053-478-1310

Email: royhaya@ipc.shizuoka.ac.jp

Abstract

We investigated the dissolution process of GaSb into InSb melt by numerical simulations using finite volume method. In addition, the dissolution process was in-situ observed by X-ray penetration method. Rectangular shaped GaSb (seed)/InSb/GaSb (feed) sandwich structure of sample was considered for the numerical analysis and the same structure of sample was used for X-ray penetration experiment. The numerical and experimental results were comparatively analyzed. From the results, it was found that the quantity of dissolved GaSb seed (at the low temperature region) was larger than that of feed (at the high temperature region). The numerical simulation results were well supported for the experimental results. Both the experiment and simulation provide deep insight into the dissolution process and composition profile in the solution during the dissolution process of ternary alloy semiconductor crystal growth.

PACS: 78.70.Ck; 81.10.-h; 81.10.Dn; 8.10.Mx

Keywords: A1. Convection; A1. Diffusion; A2. Growth from solutions; B1. Gallium compounds; B2. Semiconducting III-V materials

1. Introduction

$In_xGa_{1-x}Sb$ is one of the promising III-V ternary alloy semiconductors, which is highly useful for optoelectronic devices as well as thermo photovoltaic applications. Furthermore, $In_xGa_{1-x}Sb$ alloys show a promising performance for near-infrared detectors. By varying the Indium composition, one can vary the wavelength of detection from 1.7 to 6.8 μm [1]. However, heat and solute transport strongly affects crystal growth and it makes difficult to obtain high quality homogeneous $In_xGa_{1-x}Sb$ alloy crystals [2]. Thus, it is highly imperative to understand the complex heat and solute transport phenomena during high temperature growth process. In-situ observation during high temperature solution growth of $In_xGa_{1-x}Sb$ crystal provides deep insight into the heat and solute transport mechanism, which leads to improvements in the crystal growth and the resulting materials. Moreover, to grow a homogeneous $In_xGa_{1-x}Sb$ crystal, online monitoring of the dissolution process, composition profile in the solution, growth process and the shape of the solid-liquid interface are indispensable. Subsequently, a technique to observe the dissolution and growth processes of high temperature solution growth is required.

Techniques for in-situ observation of high temperature growth process include laser interferometry technique [3, 4], X-ray radiography [5], near infrared microscopic interferometer [6, 7], spectral reflectance [8-10], spectroscopic ellipsometry [11-14] and

X-ray fluorescence spectrometer [15, 16]. Each of these techniques is sensitive to different kind of material. For example, laser interferometry technique can be used to in-situ observation of crystal growth process in aqueous solution. However, it cannot be used for in-situ observation of composition profile change in the metallic solutions since the light cannot penetrate into it. Several numbers of reports are available in the literature for the in-situ observation of growth process of Si [17-21] as well as various binary materials [22-27]. However, only very few works were reported on the in-situ observation [9, 28] and numerical investigation [29, 30] of high temperature growth process of ternary alloy semiconductor materials. When compared to binary materials, the dissolution process and growth kinetics are more complicated for ternary materials. As a consequence, more investigations are needed to understand the dissolution and growth kinetics of ternary alloy semiconductors.

In our previous report, we have investigated the dissolution process of GaSb into InSb melt and the composition profile changes during the dissolution process of the In-Ga-Sb solution using a rectangular shaped GaSb/InSb/GaSb sandwich sample by in-situ X-ray penetration method [31]. The dissolution mechanism was discussed only based on the penetrated X-ray intensity. Thus, it needs further investigations to understand the mechanism why the dissolution of seed is much higher compare to feed

despite of high temperature at the feed end. In the present study, we performed the numerical simulations in addition with the in-situ observation experiment and the results were discussed comparatively. From the results, we have made clear the effect of solutal convection caused by the density gradient on the dissolution process.

2. Numerical Simulations

Fig. 1(a) shows the sample configuration which is used for the experimental method. The preparation of the ampoule and their dimensions were discussed in the previous article [31]. Fig. 1(b) shows the configuration and coordinate system used for the numerical analysis. The sample dimensions were fixed as 6×6×3 mm^3 (W x L x H) of GaSb seed and feed, and 6×3×3 mm^3 of InSb for the experiment. For the numerical calculation, the two dimensional symmetric rectangular model which contains the half zone of the ampoule was considered. Therefore, the sample dimensions were fixed as 3×6×3 mm^3 (W x L x H) of GaSb seed and feed, and 3×2×3 mm^3 of InSb melt for the calculation. The length of the InSb crystal was 3 mm for the experiment, where as 2 mm of InSb melt was considered for simulation due to the reduction of volume after the melting and the simulation was started when the InSb was melted. The thickness of BN and quartz are 2 mm and 1 mm which are the same dimensions of the experiment. The

calculation area was divided into 120 (x-axis) and 200 (y-axis) segments. Fig. 1(c) shows the temperature gradient used for numerical analysis. The temperature gradient at the outside of the quartz ampoule was 1°C/mm. T_L and T_H indicate the lowest and highest temperatures at the quartz tube, respectively. Table.1 shows the standard values used for the numerical calculation.

In the simulation, following assumptions have been made: (i) the liquid is incompressible and Newtonian, (ii) Boussinesq approximation. For the numerical analysis of dissolution process, the governing equations are continuity (eq.1), Navier-stokes (eq.2), Energy (eq.3) and Diffusion (eq.4) equations in liquid phase. The boundary conditions in the solution/crystal interfaces are heat balance equation (eq.6) and mass balance equation (eq.7).

The governing equations in the solution are as follows:

$$\nabla \cdot \vec{V} = 0 \tag{1}$$

$$\frac{\partial \vec{V}}{\partial t} + \left(\vec{V} \cdot \nabla\right)\vec{V} = -\nabla P + \nabla^2 \vec{V} + Gr_T T + Gr_C C \tag{2}$$

Where, $Gr_T = \dfrac{\beta_T \cdot g \cdot \Delta T \cdot L^3}{\nu^2}$ and $Gr_C = \dfrac{\beta_C \cdot g \cdot \Delta C \cdot L^3}{\nu^2}$

$$\frac{\partial T}{\partial t} + \left(\vec{V} \cdot \nabla\right)T = \frac{1}{Pr}\nabla^2 T \quad \text{Where,} \quad Pr = \frac{\nu}{\alpha} \tag{3}$$

$$\frac{\partial C}{\partial t} + \left(\vec{V} \cdot \nabla\right)C = \frac{1}{Sc}\nabla^2 C \quad \text{Where,} \quad Sc = \frac{\nu}{D} \tag{4}$$

The governing equation for the crystal and ampoule is the following heat conduction equation (eq.5):

$$\frac{\partial \mathrm{T}}{\partial \mathrm{t}} = \frac{\alpha_{\mathrm{SL,SA}}}{\mathrm{Pr}} \nabla^2 T \qquad (5)$$

Here, $\vec{\mathrm{V}}$ is the velocity vector, t the time, ρ the density, p the pressure, ν the kinematic viscosity, g the gravitational acceleration, α the thermal diffusivity, T the temperature and D, the diffusion coefficient. β_T and β_C are the thermal and solutal expansion coefficients, respectively. The subscripts S, L and A are solid, liquid, and ampoule, respectively.

Boundary conditions in the solution/crystal interface are given as follows:

(i) Heat balance equation:

$$\rho_S L \frac{\partial f}{\partial t}\left(n \cdot e_y\right) = \lambda_S \left(n \cdot \nabla T\right)_S - \lambda_L \left(n \cdot \nabla T\right)_L \qquad (6)$$

(ii) Mass balance equation:

$$\left(C_L - C_S\right)\frac{\partial f}{\partial t}\left(n \cdot e_y\right) = -D_L \left(n \cdot \nabla C\right)_L \qquad (7)$$

Here L is the latent heat, C_L is the mass fraction of GaSb in the liquid and C_S is the mass fraction of GaSb in the solid.

In order to relate these equations the liquidus curve in the InSb-GaSb pseudo-binary phase diagram was used. The governing equations and the associated boundary conditions were transformed to non dimensional equations, and the boundary fixing

method was personalized to the equations to handle the difficulties associated with curved interfaces. The above equations were solved by Finite volume method.

3. In-situ observation experiment

Rectangular shaped GaSb(seed)/InSb/GaSb(feed) sandwich structured sample with dimensions of 6 × 6 × 3 mm^3 (GaSb seed and feed) and 6 × 3 × 3 mm^3 (InSb) was used for the experiment. The samples were polished with alumina abrasive powder and etched in an acid mixture of HNO_3:HF:CH_3COOH (1:1:1) to remove the oxide layer. The sandwich sample covered by BN tube was inserted into the quartz ampoule and the ampoule was evacuated about 10^{-4} Pa before sealing. The sealed ampoule was fixed into the furnace vertically. The inside temperature profile at the centre of the ampoule was measured by using a dummy sample with a central hole along the growth axis. The inside temperatures of lower seed end and upper feed end were measured as 525.2 °C and 581.7 °C with respect to the reference temperature 650 °C. The temperature gradient at the sample position was fixed as 3.7°C/mm. The temperature of the furnace was monitored by the reference temperature which was recorded by the thermocouple connected at the middle of the furnace. Since the sample was covered by the BN tube and

quartz ampoule, the sample temperature would be reasonably varied from the reference temperature.

The furnace was fixed on a platform, which can be moved along the three directions x, y, z and can be rotated along the 360°. X-ray with an acceleration voltage of 150 kV and the current of 0.1 mA was allowed to penetrate through the sample and the penetrated X-ray intensity was recorded by a detector. The detector was a rectangular shape CdTe line sensor which had 64 cells in x-direction and 1510 cells in y-direction. The composition of the solution was measured by making the calibration line between the penetrated X-ray intensities of the standard samples of GaSb and InSb. During the experiment, the distance from the X-ray source to the sample and from the sample to the detector was fixed as 315 mm and 815 mm, respectively. As a result, the image of the sample was magnified about 2.58 times on the detector. Since each cell size of the detector was 0.1 mm, the resolution of the detector was about 0.038 mm. The temperature of the furnace was raised up to 650 °C and it was maintained constant for 1 hr 20 min. The penetrated X-ray intensities were continuously recorded for every one second to precisely observe the melting and dissolution processes.

4. Results and discussion

Figs. 2 (a)-(f) shows the numerical and experimental results of the dissolution process as a function of time. The subdivisions (i) and (ii) indicate the numerical and experimental results, respectively. In the simulated results, the streamline of the left side indicates the velocity vector of natural convection and the streamline of the right side indicates the distribution of GaSb concentration in the solution. Fig. 2(a) shows the numerical and experimental results at t=0 min. The initial time (t=0) was considered as the completion of InSb melting and the GaSb seed and feed were ready to dissolve. Initially at t=0 min, the solute concentration and the velocity of the convection flow was zero. Since, InSb was just melted at its melting temperature and the GaSb seed and feed were not yet started to dissolve into the InSb melt. As shown in Fig. 2(a) (ii), the molten InSb was easily distinguishable from the GaSb seed and feed. Since the InSb was more denser than GaSb solid, the penetrated X-ray intensity was small in the InSb region, which caused dark image in the InSb region compare to GaSb seed and feed regions. Fig. 2(b) shows the numerical and experimental results at t=0.5 min. The maximum velocity of the convective flow, V_{max} = 3.57 mm/s. The GaSb dissolved from the lower region moved towards the feed-interface due to its smaller density and it enhanced the solutal convection with high velocity. It clearly shows that the solutal convection was moved up

to high temperature region and it went down to low temperature region. Therefore, the concentration of GaSb near the feed-interface was higher than seed-interface. The numerical results clearly demonstrate that the dissolution of GaSb seed into the InSb melt. In the in-situ observation experiment, as can be seen from the Fig. 2(b) (ii), it was obvious that the dissolution of GaSb from the seed-interface as well as from the feed-interface were started. The concentration of GaSb in the solution was increased as the dissolved amount of GaSb increased in the InSb melt. The GaSb concentration contour (Fig. 2(b)(i)) clearly indicates that the solutal convection was dominant at the seed-interface when compare to the feed-interface.

Figs. 2(c)-(d) shows the numerical and experimental results at t=1 min and 2 min, respectively. The maximum velocity of convective flow at t=1 min and t=2 min were V_{max} = 2.35 mm/s and V_{max} = 1.17 mm/s, respectively. The velocity of the convective flow decreased and the concentration of the GaSb in the solution increased with time. The variation of maximum velocity of convective flow as a function of time is shown in Fig. 3. It clearly indicates that the convective flow was dominant in the beginning of dissolution at the seed-interface and became weak due to the deficiency of InSb at the seed-interface. Once the convective flow became weak, the dissolved GaSb at the feed-interface and/or transported GaSb from the seed-interface were diffused from the

feed-interface to the seed-interface in the solution. Therefore, the GaSb concentration increased in the solution. However, GaSb concentration near the feed-interface was higher than seed-interface. Thus, although the velocity of the solutal convection decreased with time, the solutal convection was still dominant in the dissolution process. From Fig. 2(c) (ii) and 2d (ii), it was clearly observed that the dissolution of GaSb from the seed-interface was increased with time. On the other hand, dissolution of GaSb from the feed-interface was suppressed. It can be clearly seen in Fig.2(c)(ii) and 2(d)(ii) that the dark region was spread towards seed end, whereas the dark region was not moved towards feed end. This is due to that large amount of dissolved GaSb solutes at the seed-interface were transported to the feed-interface mainly by buoyancy solutal convection as evidenced from simulation (Fig. 2(c) (i)), and the solute transport suppressed the further dissolution of GaSb feed at high temperature region. The solutal convection due to the density differences and thermal convection due to the temperature gradient are having an opposing effect. However, density of a solution at the high temperature is smaller than that at the low temperature and hence the convective instability due to the temperature gradient is small. It indicates that solutal convection was dominant than the thermal convection throughout the solute transport process. Therefore, the dissolved length of GaSb seed was higher than that of GaSb feed.

Figs. 2(e) and (f) show the numerical and experimental results at t=3 min and t=5 min, respectively. The velocity of convective flow at t=3 min and t=5 min was V_{max}=0.81 mm/s and V_{max}=0.38 mm/s, respectively. It clearly indicates that convective flow became weak as the time increased. On the other hand, GaSb concentration was increased in the solution due to diffusion process. Therefore, GaSb concentration in the solution approached the equilibrium value. It clearly indicates that diffusion process was dominant in the solute transport due to low velocity flow of solutal convection. From Fig. 2(e) (ii) and Fig. 2(f) (ii), it was clearly shown that the dissolution rate of GaSb at the seed-interface was decreased as a function of time since the availability of InSb solvent was decreased at the seed end. Subsequently, the dissolution was almost stopped at the seed interface as the dark region was not further shifted towards the seed end. As a result, concentration of GaSb in the solution increased with time mainly by diffusion from feed-interface. The X-ray image is not axisymmetric as the numerical calculation imposed. The asymmetric nature of X-ray image is probably due to the slight inhomogeneity of temperature inside the ampoule was reflected in the X-ray image.

The numerical simulation and experimental results clearly indicate that the solutal convection was more dominant at the beginning of dissolution process and it became weak as the time increased (Fig. 3). On the other hand, the diffusion process was

dominant at the later stage especially in the solute transport towards seed region. As a consequence of solute transport from feed-interface to seed-interface mainly by diffusion process, the solution near the undissolved seed-interface got supersaturated, which provided the necessary driving force to initiate the growth from seed interface.

Fig. 4 shows the minimum (solid line) and maximum (dotted line) GaSb concentrations in the solution as a function of time. Initially, the difference between the maximum and minimum of GaSb concentration in the solution was quite large. This is probably due to solute transport from seed-interface to feed-interface by solutal convection with high flow velocity. As a result, large amount of InSb was existed in the solution near the seed interface, which enhanced the dissolution of seed until the solution got saturated. Therefore, the difference between the maximum and minimum of GaSb concentration was higher in the initial stage. In the later stage, the difference between the maximum and minimum of GaSb concentration in the solution was decreased with increasing time. Since the velocity of the solutal convective flow decreased with time, the diffusion process became dominant and the solutes were transported towards seed-interface by diffusion. In other words, the GaSb in the solution was initially transported towards the high temperature region (feed end) by strong solutal convection and in the later stage it was distributed in the solution by diffusion process. Subsequently,

the difference between the maximum and minimum of GaSb concentration in the solution reached the steady state. It clearly indicates that the dissolved GaSb distributed in the solution by solutal convection as well as by diffusion. The experimental and numerical results demonstrate that the distribution of GaSb concentration in the solution during the dissolution process of ternary alloy semiconductor crystal growth.

Fig. 5 shows the comparison of experimental and numerical dissolution length of GaSb as a function of time. The triangular and rectangular points show the experimentally measured dissolution length of GaSb seed and feed, respectively. The solid and dotted lines indicate the simulated dissolution length of GaSb seed and GaSb feed, respectively. The interface position continuously changed as the dissolution increases. By measuring the change in distance of the interface positions with respect to the time, the dissolution length of GaSb seed and feed were obtained as a function of time. The centre point of the sample was used for the measurement. The dissolution lengths of GaSb seed and feed were increased with time. However, the dissolution rate of GaSb was decreased with time. Because, the solutal convection was dominant at the initial stage of dissolution process and it became weak as the time increased. Few minutes later, the diffusion process was dominant in the solute transport from feed-interface to seed-interface. Therefore, the dissolved length of GaSb was increased with time and

dissolution rate of GaSb was decreased with time until the solution became saturated. The results indicate that the dissolution length of GaSb seed was larger than GaSb feed even though the temperature at the seed end was smaller than feed end. From the in-situ X-ray penetration method, we observed the dissolution process of GaSb into InSb melt. The dissolution length of GaSb seed obtained by the numerical method was well agreed with the experimental data. On the other hand, the dissolution length of GaSb feed obtained by the numerical method was slightly deviated from the experimental data. For the numerical simulation, the temperature gradient was fixed as 1°C /mm at the outside of the quartz ampoule. However, in real case the inside temperature gradient of the ampoule was relatively differed from the outside temperature gradient. This may be one of the possible reasons for the slight discrepancy in the feed dissolution length. However, the tendency of the dissolution lengths of GaSb seed and feed obtained by simulated result was quantitatively agreed with the experimental results. From the experimental and simulation results, it is evident that the dissolution process of GaSb into InSb melt was strongly influenced by gravity induced solutal convection.

5. Conclusion

The effect of solutal convection and diffusion on the dissolution process of GaSb into InSb melt was investigated by numerical simulation and in-situ X-ray penetration method. Rectangular shaped GaSb (seed)/InSb/GaSb (feed) sandwich sample was used for the investigation. From the numerical and experimental results, it was found that the dissolution of GaSb seed at the low temperature region was larger than GaSb feed at the high temperature region. Since, the dissolved GaSb from the seed-interface were moved towards the feed-interface due to its smaller density and the accumulation of solutes at the feed-interface suppressed further dissolution of GaSb feed and enhanced the dissolution of GaSb seed. Numerical simulation results were agreed with the experimental results. It clearly indicates that the solute transport in the solution at initial stage was strongly influenced by solutal convection and it became diffusion dominant.

Acknowledgement

The part of the work was supported by the cooperative research projects of the Research Institute of Electronics, Shizuoka University. This work was also financially supported by a Grant-in-Aid for Scientific Research (B) (no.22360316) and a

Grant-in-Aid for Young scientist B (no. 22760005) from the Ministry of Education, Culture, Sports, Science and Technology of Japan.

References:

[1] N. Murakami, K. Arafune, T. Koyama, M. Kumagawa, Y. Hayakawa, J. Cryst. Growth **275** (2005) 433.

[2] P.S. Dutta, A.G. Ostrogorsky, J. Cryst. Growth **194** (1998) 1.

[3] K. Tsukamoto, in: I. Sunagawa (Ed.), Morphology and Growth Unit of Crystals, Terra Scientific Publishing Company, 1989, pp. 451- 478.

[4] K. Tsukamoto, E. Yokoyama, S. Maruyama, K. Maiwa, K. Shimizu, R.F. Sekerka, T.S. Morita, S. Yoda, J. Jpn. Soc. Microgravity Appl. **15** (1998) 2.

[5] K. Kakimoto, M. Eguchi, H. Watanabe, T. Hibiya, J. Cryst. Growth **91** (1988) 509.

[6] Y. Inatomi, K. Kuribayashi, Cryst. Res. Technol. **38**, (7-8), (2003) 535.

[7] Y. Inatomi, K. Kikuchi, R. Nakamura, K. Kuribayashi, I. Jimbo, J. Cryst. Growth **275** (2005) 193.

[8] R.M. Biefeld, A.A. Allerman, S.R. Kurtz, K.C. Baucom, J. Cryst. Growth **195** (1998) 356.

[9] C.J. Vineis, C.A. Wang, K.F. Jensen, W.G. Breiland, J. Cryst. Growth **195** (1998) 181.

[10] W.G. Breiland, K.P. Killeen, J. Appl. Phys.**78** (1995) 6726.

[11] W. Richter, Appl. Phys. **A 75** (2002) 129.

[12] G.N. Maracas, J.L. Edwards, D.S. Gerber, R. Droopad, Applied Surface Science **63** (1993) 1.

[13] Walter M. Duncan, Steven A. Henck, Applied Surface Science **63** (1993) 9.

[14] Y.T. Kim, R.W. Collins, K. Vedam, Surface Science **233** (1990) 341.

[15] T. Ujihara, G. Sazaki, S. Miyashita, N. Usami, K. Nakajima, Jpn. J. Appl. Phys. **39** (2000) 5981.

[16] T. Ujihara, K. Fujiwara, G. Sazaki, N. Usami, K. Nakajima, J. Cryst. Growth **242** (2002) 313.

[17] K. Fujiwara, K. Nakajima, T. Ujihara, N. Usami, G. Sazaki, H. Hasegawa, S. Mizoguchi, K. Nakajima, J. Cryst. Growth **243** (2002) 275.

[18] H. Nishizawa, F. Hori, R. Oshima, J. Cryst. Growth **236** (2002) 51.

[19] T. Aoyama, K. Kuribayashi, Acta Mater. **48** (2000) 3739.

[20] K. Fujiwara, Y. Obinata, T. Ujihara, N. Usami, G. Sazaki, K. Nakajima, J. Cryst. Growth **262** (2004) 124.

[21] X. Huang, S. Uda, H. Tanabe, N. Kitahara, H. Arimune, K. Hoshikawa, J. Cryst. Growth **307** (2007) 341.

[22] A. Tanaka, N. Izumi, M. Kimura, T. Sukegawa, J. Cryst. Growth **208** (2000) 33.

[23] G. Sazaki, Y. Azuma, S. Miyashita, N. Usami, T. Ujihara, K. Fujiwara, Y. Murakami, K. Nakajima, J. Cryst. Growth **236** (2002) 125.

[24] Y. Azuma, N. Usami, T. Ujihara, G. Sazaki, Y. Murakami, S. Miyashita, K. Fujiwara, K. Nakajima, J. Cryst. Growth **224** (2001) 204.

[25] N. Usami, Y. Azuma, T. Ujihara, G. Sazaki, S. Miyashita, Y. Murakami, K. Nakajima, Jpn. J. Appl. Phys. **40** (2001) 4141.

[26] Y. Yamauchi, N. Kobayashi, Y. Horikoshi, Jpn. J. Appl. Phys. **30**, No.5B (1991) L918.

[27] M. Kubo, T. Narusawa, J. Vac. Sci. Technol. **B8** (4) (1990) 697.

[28] Y. Hayakawa, T. Hikida, H. Mori, A. Konno, C.H. Chen, K. Arafune, H. Kawai, T. Koyama, Y. Momose, T. Ozawa, T. Aoki, J. Cryst. Growth **310** (2008) 1487.

[29] Y. Hayakawa, Y. Okano, A. Hirata, N. Imaishi, Y. Kumagiri, X. Zhong, X. Xie, B. Yuan, F. Wu, H. Liu, T. Yamaguchi, M. Kumagawa, J. Cryst. Growth **213** (2000) 40.

[30] Y. Okano, S. Umemura, Y. Enomoto, Y. Hayakawa, M. Kumagawa, A. Hirata, S. Dost, J. Cryst. Growth **235** (2002) 135.

[31] G.Rajesh, M. Arivanandhan, H. Mori, T. Aoki, T. Koyama, Y. Momose, A. Tanaka, T. Ozawa, Y. Inatomi, Y. Hayakawa, J. Cryst. Growth **312** (2010) 2677.

Figure Captions:

Fig. 1 (a) Ampoule configuration used for experimental method, (b) ampoule configuration used for numerical method, (c) temperature gradient used for numerical method.

Fig. 2 (i) Numerical result and (ii) experimental result of dissolution process as a function of time. (a) 0 min, (b) 0.5 min, (c) 1 min, (d) 2 min, (e) 3 min and (f) 5 min.

Fig. 3 Maximum velocity of convective flow near the seed as a function of time.

Fig. 4 Minimum (solid line) and maximum (dotted line) GaSb concentrations in the solution as a function of time.

Fig. 5 Comparison of experimental and numerical dissolution lengths of GaSb as a function of time.

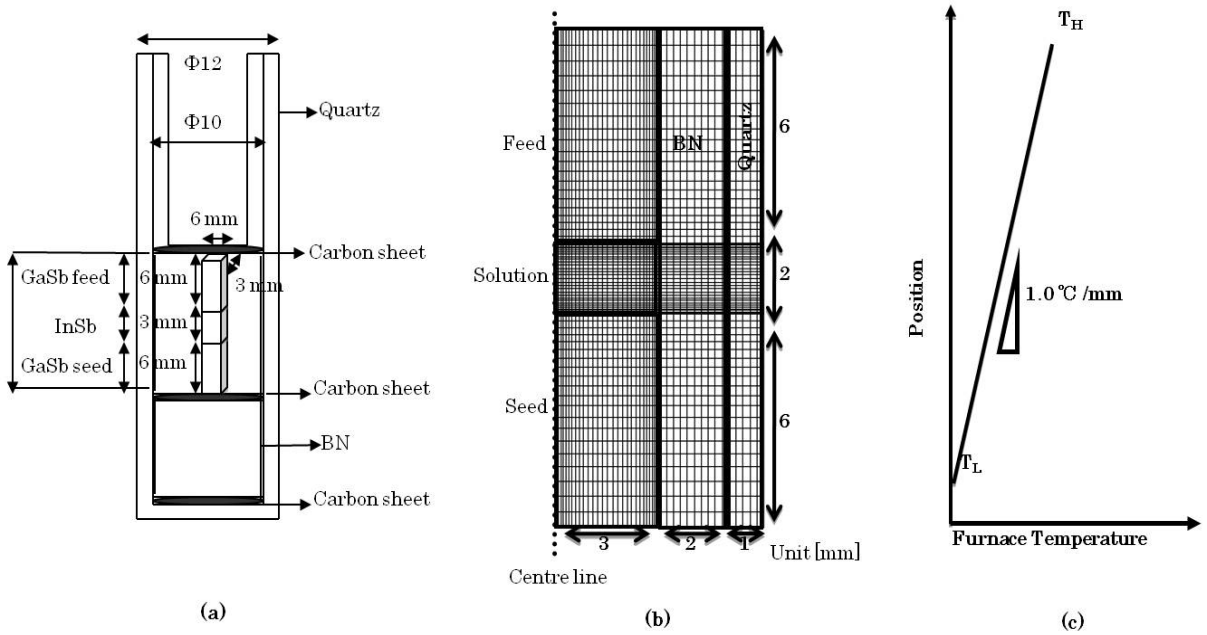
Φ12
Φ10
Quartz
6 mm
Carbon sheet
GaSb feed
6 mm
3 mm
InSb
3 mm
GaSb seed
6 mm
Carbon sheet
BN
Carbon sheet
(a)
Feed
BN
Quartz
6
Solution
2
Seed
6
3
2
1
Unit [mm]
Centre line
(b)
T_H
Position
1.0 ℃ /mm
T_L
Furnace Temperature
(c)

Fig. 1

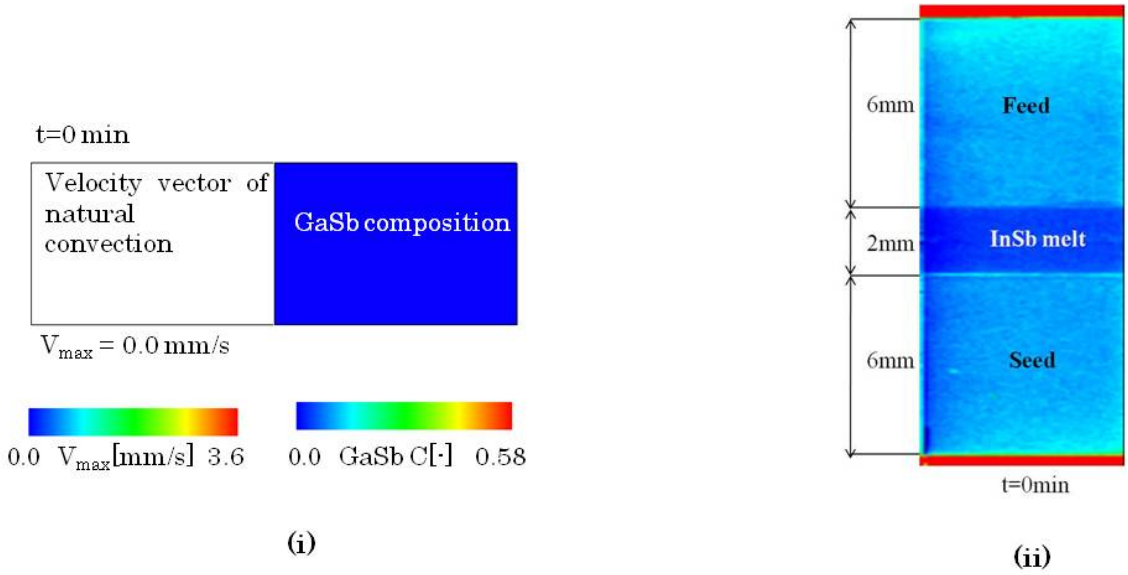
t=0 min
Velocity vector of natural convection
GaSb composition
V_{max} = 0.0 mm/s
0.0 V_{max}[mm/s] 3.6
0.0 GaSb C[-] 0.58
(i)
6mm
Feed
2mm
InSb melt
6mm
Seed
t=0min
(ii)

Fig. 2(a)

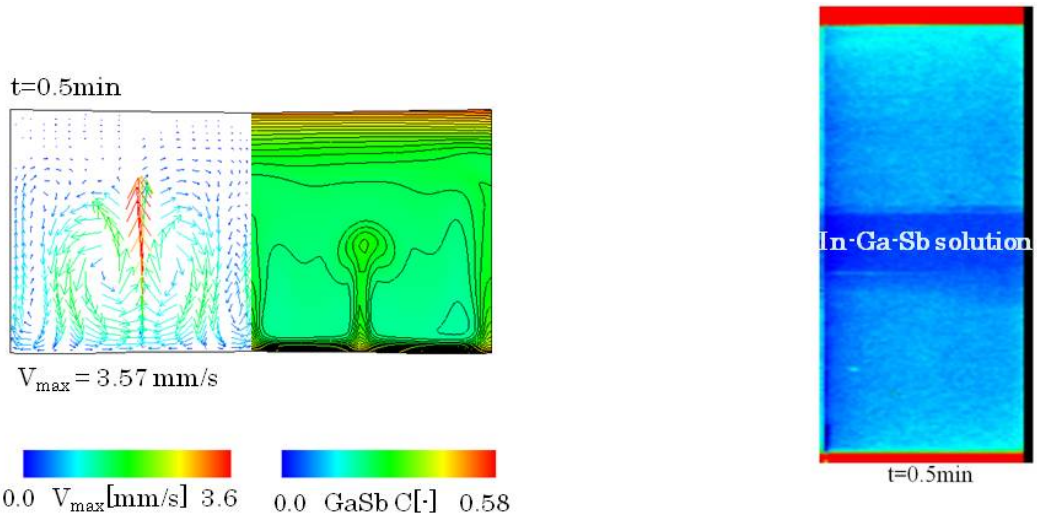
t=0.5min
V_{max} = 3.57 mm/s
0.0 V_{max}[mm/s] 3.6
0.0 GaSb C[-] 0.58
(i)
In-Ga-Sb solution
t=0.5min
(ii)

Fig. 2(b)

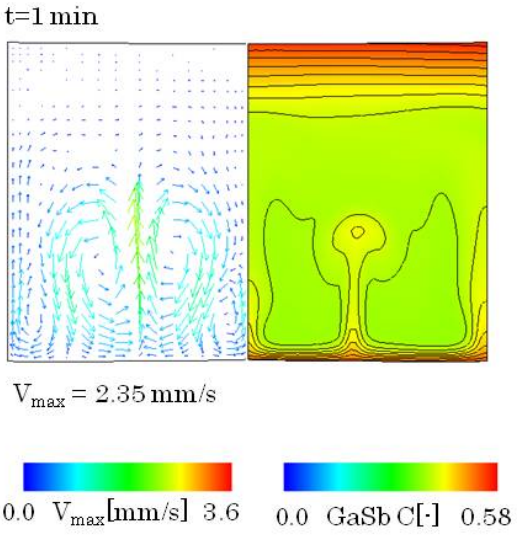

(i)

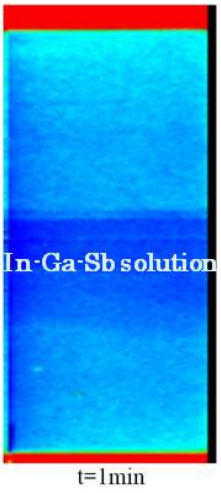

(ii)

Fig. 2(c)

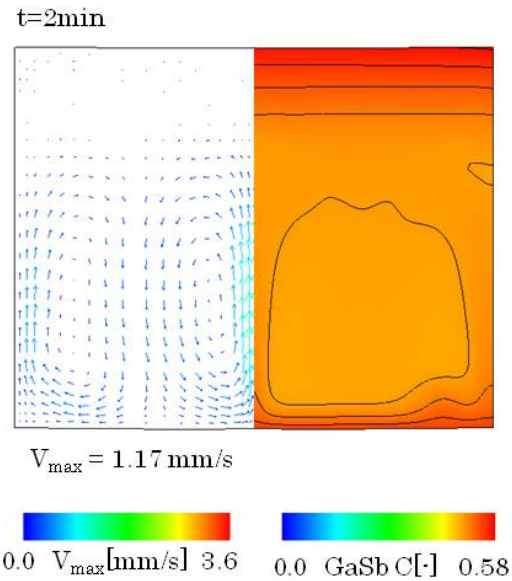

(i)

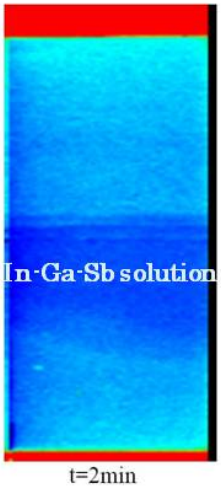

(ii)

Fig. 2(d)

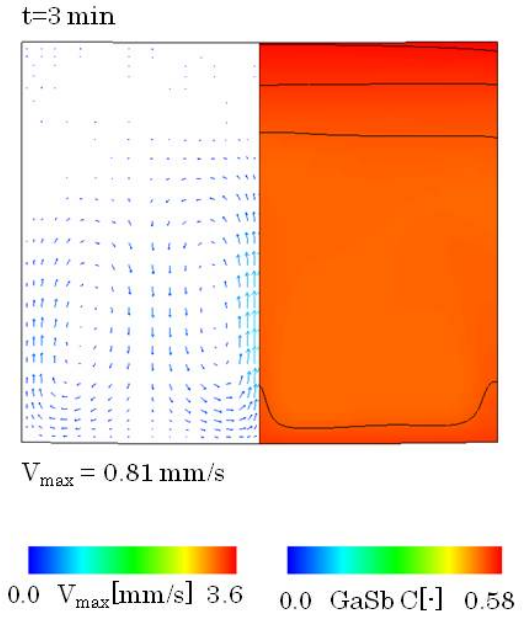

(i)

(ii)

Fig. 2(e)

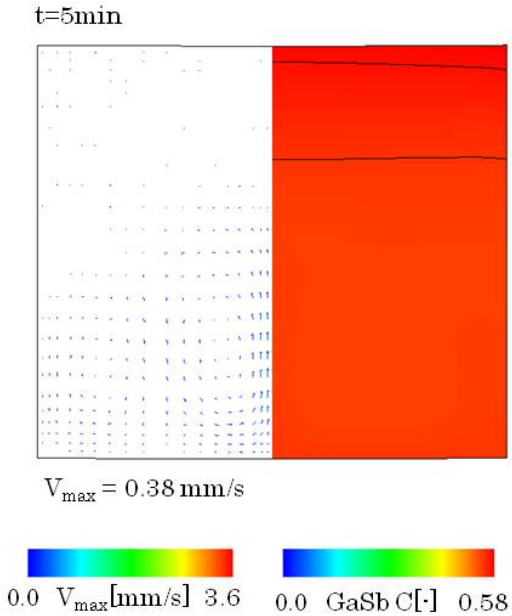

(i)

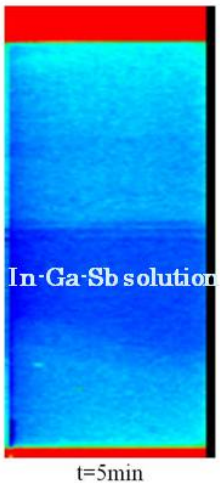

(ii)

Fig. 2(f)

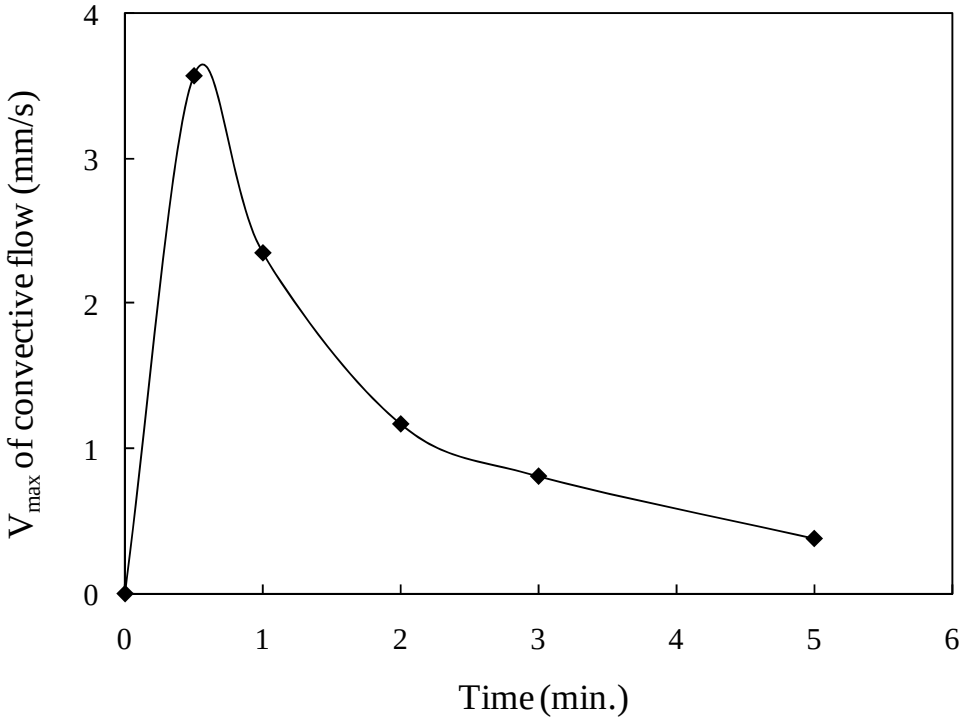

Fig. 3

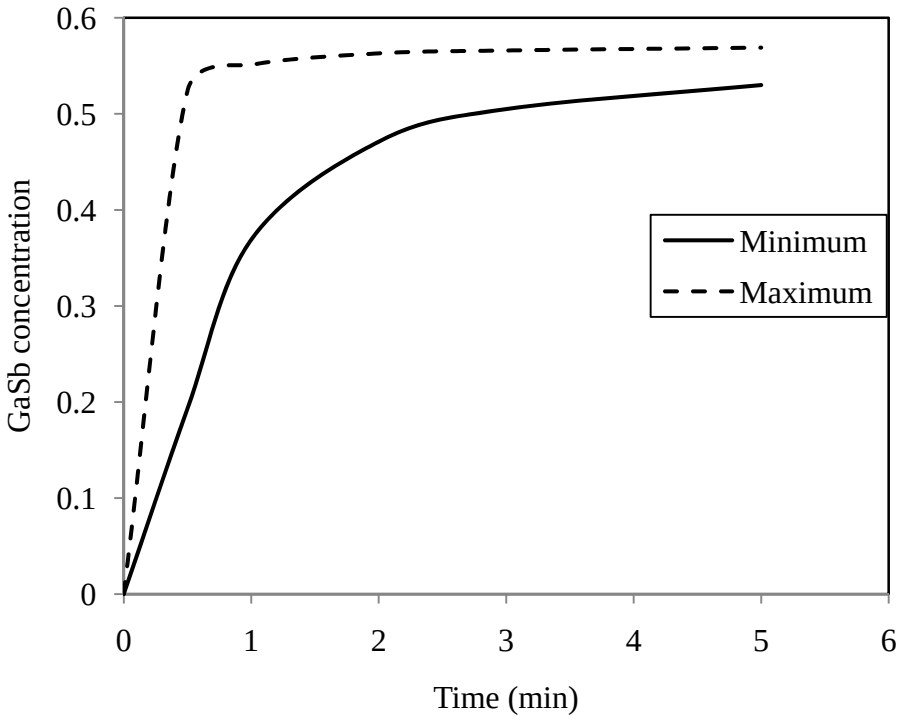
0.6
0.5
0.4
0.3
0.2
0.1
0
GaSb concentration
0
1
2
3
4
5
6
Time (min)
Minimum
Maximum

Fig. 4

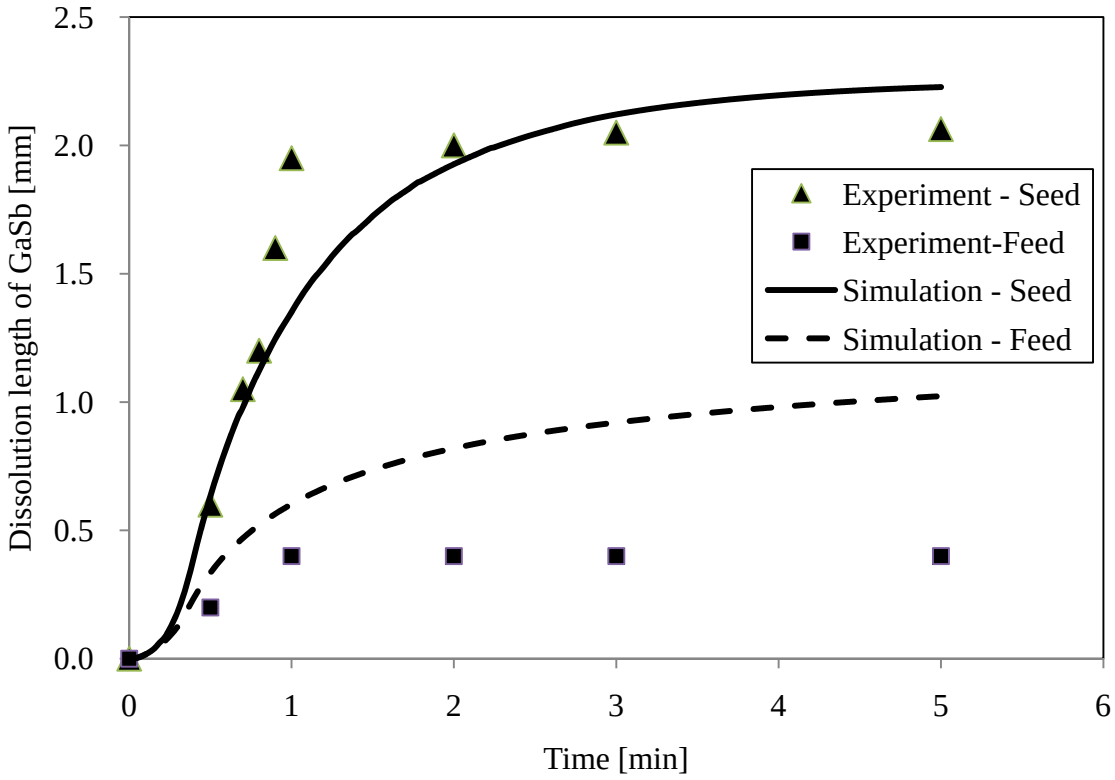
2.5
2.0
1.5
1.0
0.5
0.0
Dissolution length of GaSb [mm]
0
1
2
3
4
5
6
Time [min]
Experiment - Seed
Experiment-Feed
Simulation - Seed
Simulation - Feed

Fig. 5

Table 1 Values used for numerical calculation

Physical property	Symbol [Units]	Value
Liquid density	ρ_L [kg/m^3]	6300
Solid density	ρ_S [kg/m^3]	5600
BN density	ρ_{BN} [kg/m^3]	1900
Quartz density	ρ_Q [kg/m^3]	2200
Liquid thermal conductivity	λ_L [W/(m·K)]	17
Solid thermal conductivity	λ_S [W/(m·K)]	6.4
BN thermal conductivity	λ_{BN} [W/(m·K)]	30
Quartz thermal conductivity	λ_Q [W/(m·K)]	2.2
Liquid thermal diffusivity	α_L [m^2/s]	9.0×10^{-6}
Solid thermal diffusivity	α_S [m^2/s	3.8×10^{-6}
BN thermal diffusivity	α_{BN} [m^2/s]	8.5×10^{-6}
Quartz thermal diffusivity	α_Q [m^2/s]	1.0×10^{-6}
Liquid specific heat	$C_{p,L}$ [J/(kg·K)]	300
Solid specific heat	$C_{p,S}$ [J/(kg·K)]	300
BN specific heat	$C_{p,BN}$ [J/(kg·K)]	1850
Quartz specific heat	$C_{p,Q}$ [J/(kg·K)]	1000
Thermal expansion coefficient	β_T[K^{-1}]	1.0×10^{-4}
Solutal expansion coefficient	β_C[-]	0.05
Latent heat	ΔH [J/kg]	3.14×10^{5}
Viscosity	μ [Pa·S]	1.1×10^{-6}
Kinematic viscosity	ν [m^2/s]	1.7×10^{-7}
Diffusion coefficient	D [m^2/s]	1.2×10^{-8}